

Chapter 2

Formulation of Magnetic Field

Abstract Permanent magnet array affects flux field distribution of electromagnetic linear machines significantly. A novel dual Halbach array is proposed in this chapter to enhance the flux density in air gap, and thus to improve the output performance of linear machines. Magnetic field in 3D space of a tubular linear machine with dual Halbach array is formulated based on Laplace's and Poisson's equations. The analytical model is validated with numerical calculations from Ansoft. Furthermore, comparison of flux density between different permanent magnet arrays is done to highlight the advantages of dual Halbach array. The study shows that the employment of dual Halbach array does enhance the flux density and increase the force output of tubular linear machine. The research result in this chapter can also help the design optimization of electromagnetic linear machines.

2.1 Introduction

Electromagnetic linear machine generates linear motions directly without rotation-to-translation conversion mechanisms, which significantly simplifies system structure and improves system efficiency. It has wide applications in aeronautics [1, 2], transportation [3, 4], medical devices [5, 6] and so on. High flux density in linear machines is extremely important for applications requiring high force. The employment of permanent magnets offers electromagnetic linear machines a number of distinctive features [7] such as excellent servo characteristics and high power density. Optimized PM array is an effective way to improve flux density in linear machines. Axial and radial magnetization arrays are two of the most common arrangements of Permanent magnets. Magnet arrays with alternating magnetization directions are configured in [8] to produce radially directed flux density across the air gap of PM motors. A double-sided slotted torus axial-flux PM motor is designed for direct drive of electric vehicle in [9]. Reference [10] introduces the analysis and design of linear machines systematically. It provides a unified framework for several structure topologies. Halbach array is a promising magnet pattern due to its self-shielding property and sinusoidally distributed magnetic field in air space. It is widely applied in linear motor systems. For example, in [11], Halbach-arrayed PMs replace the

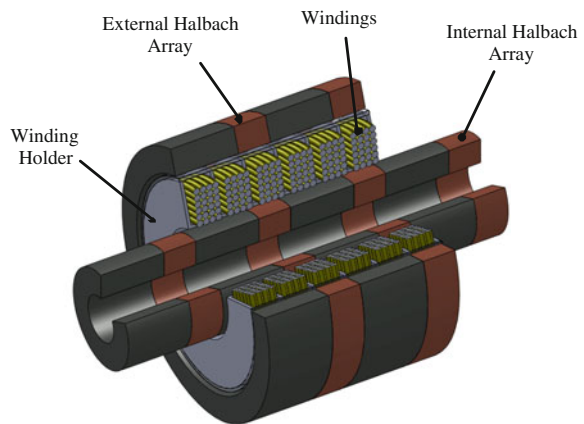
north-south magnet array in MagPie pipeline transportation system, and increase the motor propulsion force per Ampere significantly. In [12], PMs in Halbach array configuration are used for levitation, propulsion, and guidance of urban transportation systems, and achieve impressive performance. In this chapter, a tubular linear machine with dual Halbach array is proposed to further improve the magnetic flux density and thus the force output. It not only increases the radial component of flux density which is important for axial force generation, but also decreases the local force radial component which causes vibrations. Mathematical modeling of magnetic field is important for electromagnetic machines, as it could be used to predict output performance, such as flux linkage, field energy and force generation. Based on PM arrangement, magnetic field distribution in the machine is formulated with Laplace's and Poisson's equations analytically. Numerical result from finite element method is utilized to analyze and observe flux variation in three-dimensional space of the machine. The numerical result validates the analytical models. The obtained analytical model could be used for analysis of output performance and control implementation of electromagnetic linear machines with similar structures.

2.2 System Structure and Operating Principle

2.2.1 System Overall Structure

The schematic structure of the proposed PM tubular linear machine is illustrated in Fig. 2.1. The mover consists of winding phases mounted in the holds, whereas the stator is composed of dual Halbach magnet arrays that enclose the windings on internal and external sides.

Fig. 2.1 Schematic drawing of linear machines with dual Halbach array



2.2.1.1 Stator Structure

The polarization pattern of each layer of the PMs is arranged in Halbach array. As indicated in Fig. 2.2, the Halbach array consists of alternatively magnetized PMs in radial directions separated with horizontally magnetized PMs. This array offers one impressive benefit, i.e., the flux density on one side of the PMs is significantly enhanced, whereas it is self-shielded on the other side. Figure 2.2 shows that the magnetization direction for horizontal magnets in both layers is opposite, while the magnetization for radial PMs is the same. This arrangement leads to the increase of radial component of flux density in between the two layers, and the reduction of axial components. Because only the radial component of flux density can create axial force on the mover, the dual Halbach array could improve the axial force output, and reduce the radial force disturbance of linear machines. The depression of axial components helps to reduce the deformation and vibration of linear machines.

2.2.1.2 Mover Structure

Movers in electrical linear machines can be classified into two types: slotted one and slotless one. The former can usually produce high force density but also yield large force ripple due to the cogging forces. Furthermore, energy loss may exist due to the eddy current produced in the soft iron. In contrast, a slotless rotor structure eliminates the tooth ripple cogging effect and thus improves the dynamic performance and servo characteristics of linear machines, at the cost of a slight down of force output. For some particular applications such as precision manufacturing and assembly, slotless mover has greater advantages than the slotted one. Therefore, in this study, we choose the slotless type for the mover design of the linear machines.

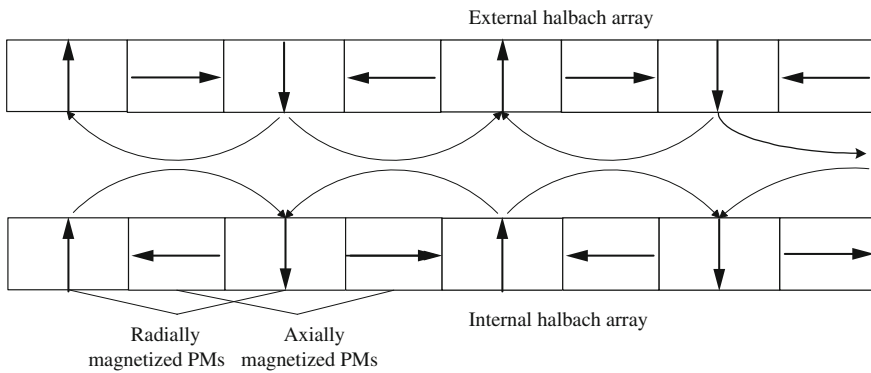


Fig. 2.2 Polarization pattern of dual Halbach array

2.2.2 *Operating Principle*

The operating principle of PM tubular linear machine with dual Halbach array is based on the Lorentz force law, i.e., force is generated by interaction between the magnetic field of PMs and the current-carrying conductors. The direction and magnitude of the force is determined by the cross product of current vector on segmental winding and magnetic flux density. Therefore, the radial component of flux density can produce forces on the mover in axial direction. The force created by the axial flux component and winding segments is symmetric around the machine axis, and thus vanishes in total. The stator and mover can be switched depending on what part we want to move for particular applications.

2.3 Governing Equations of Flux Field

Mathematical modeling of magnetic field is important for electromagnetic machines, as it could be used to predict output performance, such as flux linkage, field energy and force generation [13–15]. Generally, there are two typical ways to formulate magnetic field of electromagnetic machines, i.e., FEM [16] and magnetic equivalent circuits [17]. FEM is an efficient and accurate means to calculate magnetic field, taking full account of nonlinearity of iron material and induced currents in electrically conducting parts [18–20]. However, it is time consuming and cannot give much insight into design parameters [21]. Magnetic equivalent circuit can mainly be classified into lumped equivalent circuit and mesh-based one. The lumped equivalent circuit is the simplest approach to model the magnetic field, and allows to establish analytical relationships between design parameters and output performance. However, the technique suffers from inherent inaccuracy especially in presence of complex flux paths [22]. The mesh-based equivalent circuit is developed to achieve higher accuracy through a division of geometry [23]. However, it still requires some computational effort, although less than FEM, especially for complex models [24]. To obtain accurate knowledge of magnetic fields that directly relate motor geometry and output performance, a more sophisticated analytical field model that can compromise between accuracy and computation time is necessary [25]. Therefore, an analytical field model characterized by series expansions of the solution in terms of harmonic functions is established in this section. It will be validated by both finite element method and experiments. This approach could be applied to field modeling of other electromagnetic machines with similar magnet arrangements, and the derived parametric model is useful for analyzing the influence of parameters on output performance of electric machines.

2.3.1 Assumptions

The following assumptions are made to facilitate the subsequent study.

- The length of the linear machine is infinite, and thus the end effect of the magnetic field is ignorable.
- The magnetic permeability of back irons is infinite.
- Eddy currents in stator and mover are ignorable.

2.3.2 Magnetic Characterization of Materials

In formulation of the magnetic field, the machine space under study is divided into two regions based on magnetic characteristics. The air or coil space that has a relative permeability of 1.0 is denoted as Region 1. The permanent magnet volume filled with rare-earth magnetic material is denoted as Region 2. The back irons assumed infinite permeability is utilized to reduce magnetic energy loss, and enhance the flux density. The magnetic field property of Region 1 and 2 is characterized by the relationship between magnetic field intensity, \mathbf{H} (in A/m), and flux density, \mathbf{B} (in Tesla), as

$$\mathbf{B}_1 = \mu_0 \mathbf{H}_1, \quad (2.1)$$

$$\mathbf{B}_2 = \mu_0 \mu_r \mathbf{H}_2 + \mu_0 \mathbf{M}, \quad (2.2)$$

where μ_0 is the permeability of free space with a value of $4\pi \times 10^{-7}$ H/m, μ_r the relative permeability of Permanent magnets, $\mathbf{M} = \mathbf{B}_{rem}/\mu_0$ the residual magnetization vector in A/m, and \mathbf{B}_{rem} the remanence.

2.3.3 Governing Equations

The governing equations of magnetic field, i.e. Laplace's and Poisson's equations, are significant for the solution of magnetic field. It is known that magnetic field is a solenoid field or source-free field, i.e.,

$$\nabla \cdot \mathbf{B}_i = 0, \quad (2.3)$$

where $i = 1, 2$. It can be proved that for any vector, the divergence of its curl is always equal to zero. Thus, we can have a magnetic vector potential, \mathbf{A}_i , so that

$$\mathbf{B}_i = \nabla \times \mathbf{A}_i. \quad (2.4)$$

Because the curl of any function's (f) gradient is always equal to zero, we could have

$$\nabla \times \mathbf{A}_i = \nabla \times (\mathbf{A}_i + \nabla f),$$

which indicates that \mathbf{A}_i may have multiple solutions. To uniquely determine its value, Coulomb gauge, $\nabla \cdot \mathbf{A}_i = 0$, applies as constraint. Under Coulomb gauge, we could have

$$\nabla \times \mathbf{B}_i = -\nabla^2 \mathbf{A}_i. \quad (2.5)$$

2.3.3.1 Laplace's Equation for Region 1

The combination of Maxwell's equations and Eq. (2.1) gives

$$\nabla \times \mathbf{B}_1 = \nabla \times \mu_0 \mathbf{H}_1 = \mu_0 \mathbf{J}. \quad (2.6)$$

Substituting Eq. (2.5) into (2.6) yields

$$\nabla^2 \mathbf{A}_1 = -\mu_0 \mathbf{J},$$

where \mathbf{J} (A/m²) is current density in the field. In this study, $\mathbf{J} = 0$. Therefore, the Laplace's equation for Region 1 is obtained as

$$\nabla^2 \mathbf{A}_1 = 0. \quad (2.7)$$

2.3.3.2 Poission's Equation for Region 2

The combination of Maxwell's equations and Eq. (2.2) gives

$$\nabla \times \mathbf{B}_2 = \mu_0 \mu_r \mathbf{J} + \mu_0 \nabla \times \mathbf{M}. \quad (2.8)$$

Similarly, Eqs. (2.5) and (2.8) yield the Poisson equation for Region 2

$$\nabla^2 \mathbf{A}_2 = -\mu_0 \nabla \times \mathbf{M}. \quad (2.9)$$

2.4 General Solutions to Magnetic Field

2.4.1 General Solution to Laplace's Equation

The magnetic field distribution of tubular linear machine is axially symmetric. Therefore, \mathbf{A}_i has only one component, $A_{i,\theta}$. The Laplace equation in cylindrical coordinators can be simplified as

$$\frac{\partial^2 A_\theta}{\partial z^2} + \frac{\partial}{\partial r} \left(\frac{1}{r} \frac{\partial}{\partial r} (r A_\theta) \right) = 0. \quad (2.10)$$

Since A_θ is only a function of r and θ , we assume that

$$A_\theta = R(r) Z(z). \quad (2.11)$$

Substituting into Eq. (2.10) yields

$$\frac{1}{R(r)} \frac{\partial^2 R(r)}{\partial r^2} + \frac{1}{R(r)r} \frac{\partial R(r)}{\partial r} + \frac{1}{Z(z)} \frac{\partial^2 Z(z)}{\partial z^2} - \frac{1}{r^2} = 0, \quad (2.12)$$

while r and z are independent variables, and the third term as a function of z must be a constant. So the following formula is established

$$\frac{1}{Z(z)} \frac{\partial^2 Z(z)}{\partial z^2} = k^2. \quad (2.13)$$

Then Eq. (2.12) becomes

$$\frac{1}{R(r)} \frac{\partial^2 R(r)}{\partial r^2} + \frac{1}{R(r)r} \frac{\partial R(r)}{\partial r} + k^2 - \frac{1}{r^2} = 0. \quad (2.14)$$

Equation (2.13) can then be rewritten as

$$\frac{\partial^2 Z(z)}{\partial z^2} - k^2 Z(z) = 0. \quad (2.15)$$

Thus, Laplace's equation, Eq. (2.10), is separated into two equations, i.e., Eqs. (2.14) and (2.15). There are three possible solutions to Eqs. (2.14) and (2.15) according to the variation of k .

2.4.1.1 The First Solution

When $k^2 = 0$, the following equations are obtained

$$\begin{aligned} Z(z) &= E_0 + F_0 z, \\ r^2 \frac{\partial^2 R(r)}{\partial r^2} + r \frac{\partial R(r)}{\partial r} - R(r) &= 0. \end{aligned} \quad (2.16)$$

The solution to Eq. (2.16) is

$$A_\theta = R(r) Z(z) = \left(C_0 r + D_0 \frac{1}{r} \right) (E_0 + F_0 z). \quad (2.17)$$

However, as A_θ should be a periodic function of z , Eq. (2.17) is not the valid solution of A_θ .

2.4.1.2 The Second Solution

When $k^2 > 0$, the following equation is obtained as

$$\begin{aligned} Z(z) &= E_0 e^{kz} + F_0 e^{-kz}, \\ r^2 \frac{\partial^2 R(r)}{\partial r^2} + r \frac{\partial R(r)}{\partial r} + R(r) (k^2 r^2 - 1) &= 0. \end{aligned} \quad (2.18)$$

Let $kr = x$. The second formula of Eq. (2.18) is

$$x^2 \frac{\partial^2 R}{\partial x^2} + x \frac{\partial R}{\partial x} + (x^2 - 1) R = 0.$$

The solution to Eq. (2.16) is

$$A_\theta = R(r) Z(z) = [C_0 J_1(kr) + D_0 Y_1(kr)] (E_0 e^{kz} + F_0 e^{-kz}). \quad (2.19)$$

Again, because Eq. (2.19) is not a periodic function of z , it is not the solution of Laplace's equation either.

2.4.1.3 The Third Solution

When $k^2 < 0$, the following equations are obtained

$$\begin{aligned} Z(z) &= B_0 \cos(mz) + B_1 \sin(mz), \\ r^2 \frac{\partial^2 R(r)}{\partial r^2} + r \frac{\partial R(r)}{\partial r} + R(r) (k^2 r^2 - 1) &= 0. \end{aligned} \quad (2.20)$$

Let $mr = x$, Eq. (2.20) is

$$x^2 \frac{\partial^2 R}{\partial x^2} + x \frac{\partial R}{\partial x} - (x^2 + 1) R = 0.$$

The solution to Eq. (2.20) is

$$A_\theta = R(r) Z(z) = [C_0 I_1(mr) + D_0 K_1(mr)] * [E_0 \cos(mz) + F_0 \sin(mz)], \quad (2.21)$$

where m is a real number and defined with $k = jm$. In this case, A_θ is a periodic function of z . It is probably the solution of Laplace's equation. To determine the coefficients in above equation, constraints are needed. Because the axial component of flux density is antisymmetry on $z = 0$, we have $B_z|_{z=0} = 0$. Substituting Eq. (2.21) into (2.4) gives

$$\begin{aligned} C_0 &= 0, \\ D_0 &= 0. \end{aligned}$$

Therefore, the general solution to Laplace's equation is

$$A_\theta = [a_n I_1(mr) + b_n K_1(mr)] \sin(mz), \quad (2.22)$$

where $a_n = E_0$, $b_n = F_0$.

2.4.2 General Solution to Poisson's Equation

The Poisson equation in cylindrical coordinators is

$$\frac{\partial A_\theta}{\partial z^2} + \frac{\partial}{\partial r} \left(\frac{1}{r} \frac{\partial}{\partial r} (r A_\theta) \right) = -\mu_0 \nabla \times \mathbf{M}. \quad (2.23)$$

The general solution to the corresponding homogeneous equation of the Poisson's equation is

$$A_\theta = \sum_{n=1,2,\dots}^{\infty} [a_n I_1(m_n r) + b_n K_1(m_n r)] \sin(m_n z). \quad (2.24)$$

To get the solution of Poisson equation, the right side of the equation needs to be substituted by harmonic expansion of magnetization vector. As illustrated in Fig. 2.2, the two Halbach arrays (Region 1 and Region 3) in the linear machine are composed of radial and axial magnets. The magnetization vector, \mathbf{M} , has two components M_r and M_z in r and z direction, respectively. It is given in cylindrical coordinators as

$$\mathbf{M} = M_r e_r + M_z e_z. \quad (2.25)$$

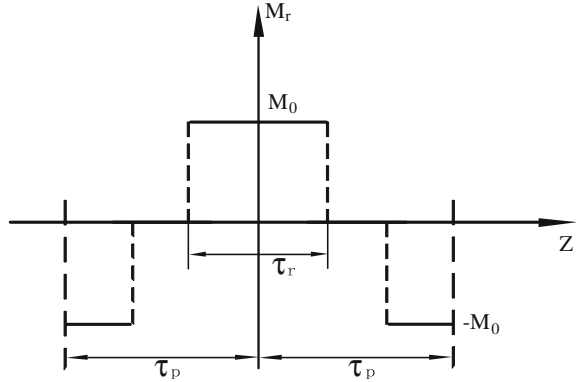
M_r is a non-continuous function with a period of $2\tau_p$, and its variation in z direction is shown in Fig. 2.3. To get the derivative of M_r , harmonic expansion is utilized,

$$M_r = \begin{cases} -M_0 & -\tau_p \leq z < \frac{\tau_r}{2} - \tau_p \\ 0 & \frac{\tau_r}{2} - \tau_p \leq z < -\frac{\tau_r}{2} \\ M_0 & -\frac{\tau_r}{2} \leq z < \frac{\tau_r}{2} \\ 0 & \frac{\tau_r}{2} \leq z < \tau_p - \frac{\tau_r}{2} \\ -M_0 & \tau_p - \frac{\tau_r}{2} \leq z < \tau_p \end{cases},$$

where τ_r is width of radial magnets and τ_p is the pole pitch. It can be expanded with Fourier series as

$$M_r = \sum_{n=1,2,\dots}^{\infty} 4 \left(B_{rem} / \mu_0 \right) \frac{\sin \left[(2n-1) \frac{\pi}{2} \alpha_p \right]}{(2n-1) \pi} \cos(m_n z), \quad (2.26)$$

Fig. 2.3 M_r as a function of z



where $\alpha_p = \frac{\tau_r}{\tau_p}$, n is positive integer, and

$$m_n = (2n - 1) \pi / \tau_p. \quad (2.27)$$

Therefore,

$$\begin{aligned} & -\mu_0 \nabla \times \mathbf{M} \\ &= \sum_{n=1,2,\dots}^{\infty} 4B_{rem} \frac{\sin[(2n-1)\frac{\pi}{2}\alpha_p]}{\tau_p} \sin(m_n z) \\ &= \sum_{n=1,2,\dots}^{\infty} P_n \sin(m_n z), \end{aligned}$$

where $P_n = \frac{4}{\tau_p} B_{rem} \sin[(2n-1)\frac{\pi}{2}\alpha_p]$. The general solution of Poisson equation is obtained

$$A_{2\theta} = \sum_{n=1,2,\dots}^{\infty} \{[a_{2n} I_1(m_n r) + b_{2n} K_1(m_n r)] \sin(m_n z) + S(r, z)\}, \quad (2.28)$$

where $S(r, z) = R(r)Z(z)$ is a particular solution of Poisson equation. Substituting $S(r, z)$ into Poisson equation gives

$$\frac{1}{R(r)} \frac{\partial^2 R(r)}{\partial r^2} + \frac{1}{R(r)r} \frac{\partial R(r)}{\partial r} + \frac{1}{Z(z)} \frac{\partial^2 Z(z)}{\partial z^2} - \frac{1}{r^2} = R(r) Z(z) P_n \sin(m_n z). \quad (2.29)$$

Let $\frac{1}{Z(z)} \frac{\partial^2 Z(z)}{\partial z^2} = -m_n^2$. It is simplified as

$$Z(z) = \sin(m_n z), \quad (2.30)$$

$$r^2 \frac{\partial^2 R(r)}{\partial r^2} + r \frac{\partial R(r)}{\partial r} - R(r) (m_n^2 r^2 + 1) = r^2 P_n. \quad (2.31)$$

Let $m_n r = x$. Equation (2.31) is reduced to

$$x^2 \frac{\partial^2 R(r)}{\partial x^2} + x \frac{\partial R(r)}{\partial x} - R(r) (x^2 + 1) = \frac{2x^2}{\pi} \frac{\pi P_n}{2m_n^2}.$$

Let $y = R(r) \frac{2m_n^2}{\pi P_n}$. The above equation becomes

$$x^2 \frac{\partial^2 y}{\partial x^2} + x \frac{\partial y}{\partial x} - y (x^2 + 1) = \frac{2x^2}{\pi}.$$

The above equation is a modified Struve equation. Its solution is

$$R(r) = \frac{\pi \text{Struve} L_1(m_n r)}{2m_n^2} P_n.$$

Therefore, the particular solution to Poisson equation is

$$S(r, z) = R(r) Z(z) = \frac{\pi \text{Struve} L_1(m_n r)}{2m_n^2} P_n \sin(m_n z), \quad (2.32)$$

where L_1 is the modified Struve functions [26] and appears as special solutions of inhomogeneous Bessel equations. As a result, the general solutions to Laplace and Poisson equations are

$$\begin{aligned} A_{1\theta} &= \sum_{n=1,2,\dots}^{\infty} [a_{1n} I_1(m_n r) + b_{1n} K_1(m_n r)] \sin(m_n z), \\ A_{2\theta} &= \sum_{n=1,2,\dots}^{\infty} \{[a_{2n} I_1(m_n r) + b_{2n} K_1(m_n r)] \sin(m_n z) \\ &\quad + \frac{1}{2} \frac{\pi \text{Struve} L_1(m_n r)}{m_n^2} P_n \sin(m_n z)\}. \end{aligned} \quad (2.33)$$

2.4.3 Solutions to Flux Density Distribution

From Eqs. (2.4), and (2.33), the general solutions of flux density is obtained

$$\begin{aligned} B_{r1} &= \sum_{n=1,2,\dots}^{\infty} -m_n [a_{1n} I_1(m_n r) + b_{1n} K_1(m_n r)] \cos(m_n z), \\ B_{r2} &= \sum_{n=1,2,\dots}^{\infty} -m_n \{[a_{2n} I_1(m_n r) + b_{2n} K_1(m_n r)] \cos(m_n z) \end{aligned}$$

$$\begin{aligned}
& + \frac{1}{2} \frac{\pi \text{Struve} L_1(m_n r)}{m_n^2} P_n \cos(m_n z)\}, \\
B_{z1} &= \sum_{n=1,2,\dots}^{\infty} m_n [a_{1n} I_0(m_n r) - b_{1n} K_0(m_n r)] \sin(m_n z), \\
B_{z2} &= \sum_{n=1,2,\dots}^{\infty} m_n \{[a_{2n} I_0(m_n r) - b_{2n} K_0(m_n r)] \sin(m_n z) \\
& + \frac{1}{2} \frac{\pi \text{Struve} L_0(m_n r)}{m_n^2} P_n \sin(m_n z)\}.
\end{aligned} \tag{2.34}$$

B_{r1} and B_{z1} represents the radial and axial magnetic field in the winding region, while B_{r2}^p and B_{z2}^p are in magnet regions. The upper script, $p = 1, 2$, represents external and internal PMs respectively.

2.4.4 Boundary Conditions

Boundary conditions are necessary to determine the specific solutions of magnetic field. In this study, boundary conditions are employed to calculate the coefficients in the expression of magnetic flux density, such as a_{in} , b_{in} . The magnetic field follows certain rules along the boundary of two different media. For example, the flux density component perpendicular to the boundary is continuous in two neighboring media, and the tangential component of magnetic intensity is discontinuous by the amount of surface current at the boundary. In this study, surface current is zero. Therefore, the tangential component of magnetic intensity is continuous. The boundary conditions are

$$\begin{aligned}
B_{1z}|_{r=R_s} &= \mu_0 M_{z1}; B_{3z}|_{r=R_r} = \mu_0 M_{z3}, \\
B_{1r}|_{r=R_b} &= B_{2r}|_{r=R_b}; H_{1z}|_{r=R_b} = H_{2z}|_{r=R_b}, \\
B_{2r}|_{r=R_a} &= B_{3r}|_{r=R_a}; H_{2z}|_{r=R_a} = H_{3z}|_{r=R_a}.
\end{aligned} \tag{2.35}$$

From the boundary conditions, the coefficients in magnetic flux density can be obtained.

2.5 Finite Element Analysis and Results

2.5.1 Overall Field Distribution

Figure 2.4 describes overall magnetic field distribution of a tubular linear machine with dual Halbach array. The major parameters used in the computation are given in Table 2.1. The magnets are sintered NdFeB with $B_{rem} = 1.2(\text{T})$ and $\mu_r = 1.0997$.

Fig. 2.4 Magnetic field distribution of machines with dual Halbach array

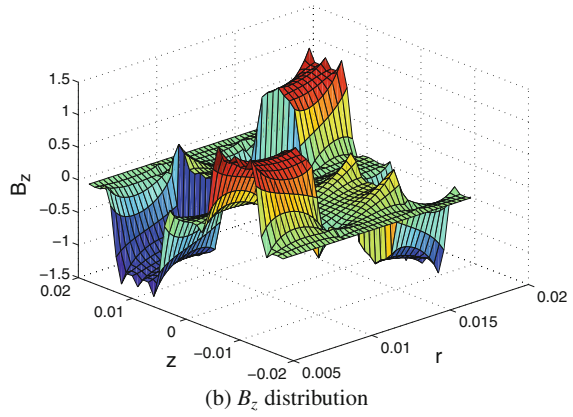
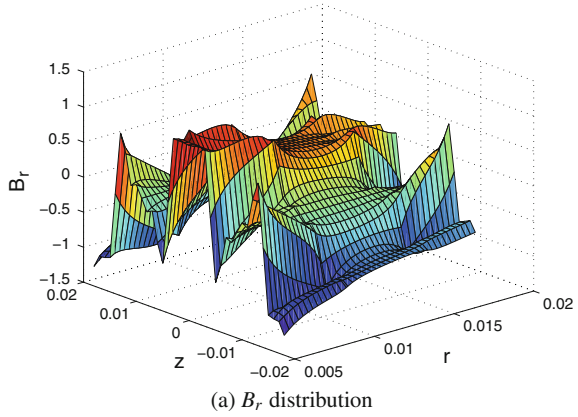


Table 2.1 Structure parameters in the numerical computations

Outer radius of external Halbach R_s	17 (mm)
Inner radius of external Halbach array R_b	14 (mm)
Outer radius of internal Halbach array R_a	9 (mm)
Inner radius of internal Halbach array R_r	5 (mm)
Pole pitch τ_p	9 (mm)
Axial width of radially magnetized PMs τ_r	18 (mm)

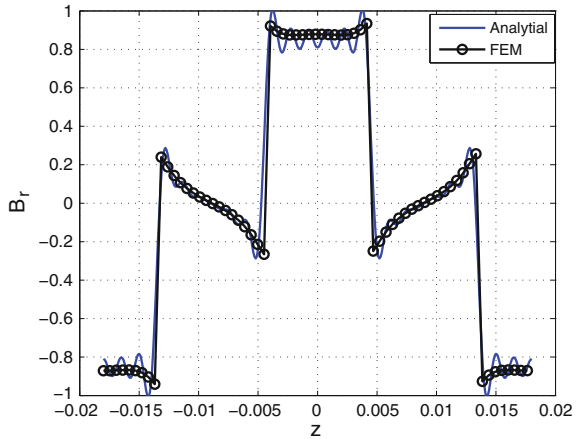
Magnetic field of a tubular linear machine is calculated with radial field B_r and axial component B_z by utilizing established analytical model. Figure 2.4a gives the variation of B_r , and Fig. 2.4b gives the variation of B_z in both magnet and winding regions. It is found that radial field is continuous in the radial direction while axial component jumps at the radial boundary of different materials. B_r and B_z variation is

consistent with the distribution of remanence M_r and M_z in the magnet region. The magnetic field in the winding region tends to be uniform. Analytical model is then validated with finite element result according to two regions denoted by materials: magnet region and winding region. As it is assumed that the machine length is infinite, the finite element solutions are obtained by applying a master–slave boundary at the axial boundaries $z = 0$, $z = \tau_p$ and imposing symmetry boundary at $z = 0$.

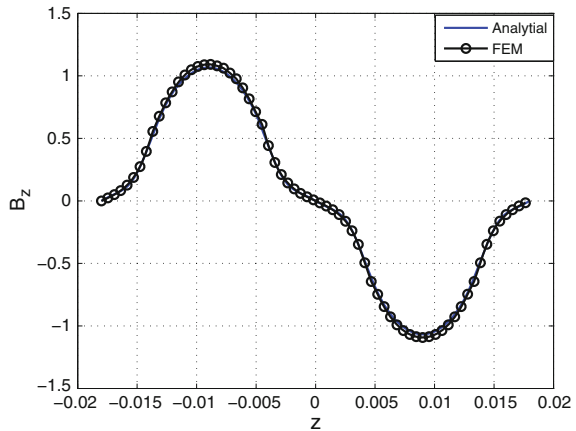
2.5.2 Magnetic Field Variation in the Magnet Region

Figures 2.5 and 2.6 show magnetic field variation versus axial distance z at the center radius of internal and external Halbach arrays, i.e., $r = (R_r + R_a)/2$ and $r = (R_b + R_s)/2$, respectively. Magnetic field in either magnet region varies in line with

Fig. 2.5 Magnetic field variation at the center of internal magnet area

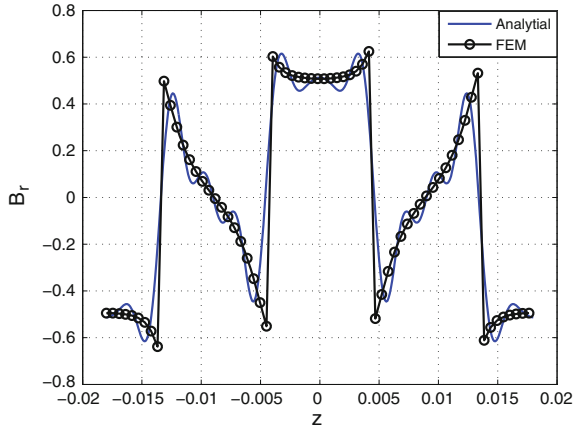


(a) B_r variation

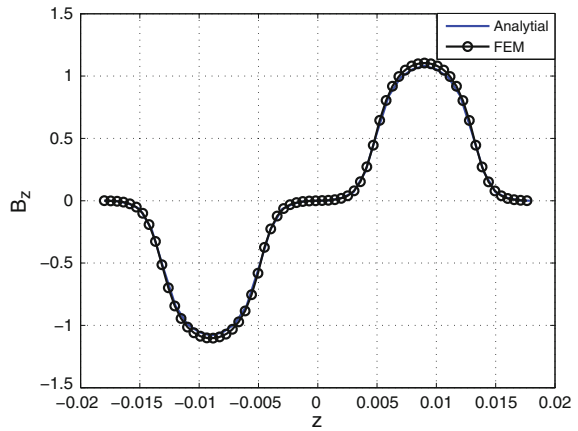


(b) B_z variation

Fig. 2.6 Magnetic field variation at the center of external magnet area



(a) B_r variation



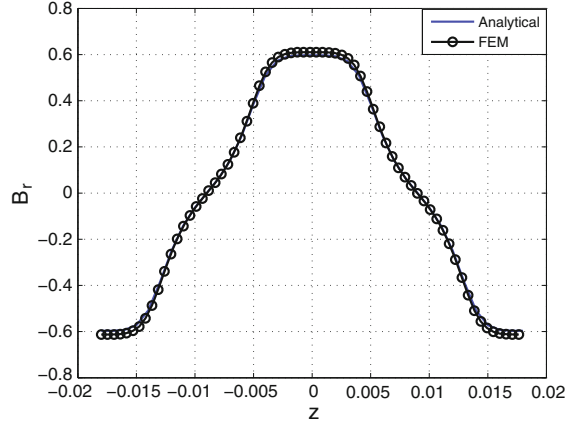
(b) B_z variation

the magnetization vector M . Therefore, the radial flux component is even-symmetric about $z = 0$ mm, while the axial field is odd-symmetric. However, the radial flux density in the internal magnet area is greater than that in the external magnet area due to a decreasing section crossed by constant flux lines. The analytical results fit with the finite element results well. The difference is mainly caused by the simplification of models and FEM meshing.

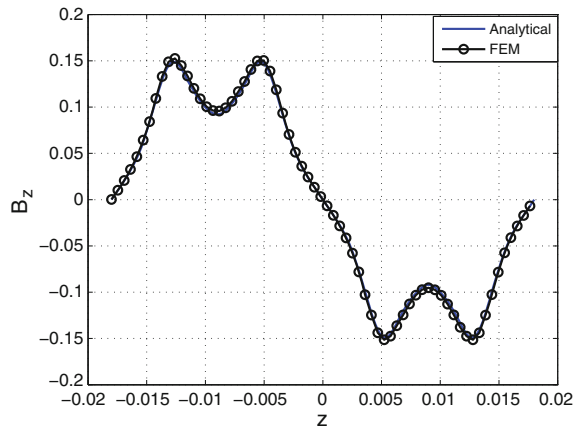
2.5.3 Magnetic Field Variation in the Winding Region

Figure 2.7 shows B_r and B_z variation versus z at a constant radius $r = 12$ mm. The radial field is severely uniform in the radial magnet region, while the axial field

Fig. 2.7 Magnetic field variation in the winding region



(a) B_r variation



(b) B_z variation

reaches peak point at the axial boundary of magnets. The radial field variation related to force output is an approximate sine waveform which makes the motion control easy. It is found that the analytical results fit well with finite element results.

The foregoing study validates the analytical model with numerical calculations in Ansoft environment. The analytical model of an infinite length motor is proved to be accurate. However, longitude fringe effect (LFE) always exists in a tubular linear machine in practice because of finite length and it is uncertain whether the established motor fit well with a practical machine measurements.

2.6 Conclusion

A novel dual Halbach array is proposed in this chapter for the development of tubular linear machines. It helps to improve the radial flux, and reduce the axial flux. The 3D magnetic field distribution is formulated analytically based on Laplace's and Poisson's equations. Numerical computation of magnetic field is conducted with FEM method. It shows that the analytical model fits with the numerical result closely. The analytical model in this chapter can be used for design optimization and control implementation of tubular electromagnetic linear machines.

References

1. Aydemir MT, Zarko D, Lipo TA (2004) Design of a linear bulk superconductor magnet synchronous motor for electromagnetic aircraft launch systems. *IEEE Trans Appl Supercond* 14(1):54–62
2. Kou B, Huang X, Wu H et al (2009) Thrust and thermal characteristics of electromagnetic launcher based on permanent magnet linear synchronous motors. *IEEE Trans Magn* 45(1):358–362
3. Thornton R, Thompson MT, Perreault BM et al (2009) Linear motor powered transportation. *Proc IEEE* 97(11):1754–1757
4. Yan L (2009) The linear motor powered transportation development and application in China. *Proc IEEE* 97(11):1872–1880
5. Yamada H, Yamaguchi M, Karita M et al (1994) Acute animal experiment using a linear motor-driven total artificial heart. *IEEE Transl J Magn Jpn* 9(6):90–97
6. Yamada H, Yamaguchi M, Kobayashi K et al (1995) Development and test of a linear motor-driven total artificial heart. *IEEE Eng Med Biol Mag* 14(1):84–90
7. Mohammadpour A, Gandhi A, Parsa L (2012) Winding factor calculation for analysis of back EMF waveform in air-core permanent magnet linear synchronous motors. *IET Electr Power Appl* 6(5):253–259
8. Wang J, Howe D (2004) Design optimization of radially magnetized, iron-cored, tubular permanent-magnet machines and drive systems. *IEEE Trans Magn* 40(5):3262–3277
9. Mahmoudi A, Rahim NA, Ping HW (2012) Axial-flux permanent-magnet motor design for electric vehicle direct drive using sizing equation and finite element analysis. *Prog Electromagn Res* 122:467–496
10. Wang J, Jewell GW, Howe D (1999) A general framework for the analysis and design of tubular linear permanent magnet machines. *IEEE Trans Magn* 35(3):1986–2000
11. Fang J, Montgomery DB, Roderick L (2009) A novel magpipe pipeline transportation system using linear motor drives. *Proc IEEE* 97(11):1848–1855
12. Gurol HS (2009) General atomics linear motor applications: moving towards deployment. *Proc IEEE* 97(11):1864–1871
13. Torkaman H, Afjei E (2009) Magnetostatic field analysis regarding the effects of dynamic eccentricity in switched reluctance motor. *Prog Electromagn Res M* 8:163–180
14. Torkaman H, Afjei E (2010) Comparison of two types of dual layer generator in field assisted mode utilizing 3D-FEM and experimental verification. *Prog Electromagn Res B* 23:293–309
15. Torkaman H, Afjei E (2012) Comparison of three novel types of two-phase switched reluctance motors using finite element method. *Prog Electromagn Res* 125:151–164
16. Jian L, Chau KT (2010) Design and analysis of a magnetic-gear electronic-continuously variable transmission system using finite element method. *Prog Electromagn Res* 107:47–61

17. Touati S, Ibtouen R, Touhami O et al (2011) Experimental investigation and optimization of permanent magnet motor based on coupling boundary element method with permeances network. *Prog Electromagn Res* 111:71–90
18. Lecointe JP, Cassoret B, Brudny JF (2011) Distinction of toothing and saturation effects on magnetic noise of induction motors. *Prog Electromagn Res* 112:125–137
19. Zhao W, Cheng M, Cao R et al (2012) Experimental comparison of remedial single-channel operations for redundant flux-switching permanent-magnet motor drive. *Prog Electromagn Res* 123:189–204
20. Mahmoudi A, Kahourzade S, Rahim NA et al (2012) Improvement to performance of solid-rotor-ringed line-start axial-flux permanent-magnet motor. *Prog Electromagn Res* 124:383–404
21. Musolino A, Rizzo R, Tripodi E (2012) Tubular linear induction machine as a fast actuator: analysis and design criteria. *Prog Electromagn Res* 132:603–619
22. Matyas AR, Biro KA, Fodorean D (2012) Multi-phase synchronous motor solution for steering applications. *Prog Electromagn Res* 131:63–80
23. Kim YH, Jin CS, Kim S et al (2002) Analysis of hybrid stepping motor using 3D equivalent magnetic circuit network method based on trapezoidal element. *J Appl Phys* 91(10):8311–8313
24. Amrhein M, Krein PT (2010) Induction machine modeling approach based on 3-D magnetic equivalent circuit framework. *IEEE Trans Energy Convers* 25(2):339–347
25. Liu C, Chau KT (2012) Electromagnetic design and analysis of double-rotor flux-modulated permanent-magnet machines. *Prog Electromagn Res* 131:81–97
26. The wolfram functions site, <http://functions.wolfram.com/Bessel-TypeFunctions/StruveL/introductions/Struves/01/>

Electromagnetic Linear Machines with Dual Halbach
Array

Design and Analysis

Yan, L.; Zhang, L.; Peng, J.; Zhang, L.; Jiao, Z.

2017, XXIII, 125 p. 90 illus., 59 illus. in color., Hardcover

ISBN: 978-981-10-2307-1